Phase Biaxiality in Nematic Liquid Crystalline Side-Chain Polymers of Various Chemical Constitutions

Kirsten Severing, Elke Stibal-Fischer, Alfred Hasenhindl, Heino Finkelmann, and Kay Saalwächter*

Institut für Makromolekulare Chemie, Universität Freiburg, Stefan-Meier-Strasse 31, D-79104 Freiburg, Germany

Received: January 25, 2006; In Final Form: June 14, 2006

In a previous deuterium NMR study conducted on a liquid crystalline (LC) polymer with laterally attached book-shaped molecules as the mesogenic moiety, we have revealed a biaxial nematic phase below the conventional uniaxial nematic phase (*Phys. Rev. Lett.* **2004**, *92*, 125501). To elucidate details of its formation, we here report on deuterium NMR experiments that have been conducted on different types of LC side-chain polymers as well as on mixtures with low-molar-mass mesogens. Different parameters that affect the formation of a biaxial nematic phase, such as the geometry of the attachment, the spacer length between the polymer backbone and the mesogenic unit, as well as the polymer dynamics, were investigated. Surprisingly, also polymers with terminally attached mesogens (*end-on polymers*) are capable of forming biaxial nematic phases if the flexible spacer is short and thus retains a coupling between the polymer backbone and the LC phase. Furthermore, the most important parameter for the formation of a biaxial nematic phase is the dynamics of the polymer backbone, as the addition of a small percentage of low molar mass LC to the biaxial nematic polymer from the original study served to shift both the glass transition and the appearance of detectable biaxiality in a very similar fashion. Plotting different parameters for the investigated systems as a function of T/T_g also reveals the crucial role of the dynamics of the polymer backbone and hence the glass transition.

Introduction

The existence of a biaxial nematic phase was predicted by Freiser as early as 1970.[1] This special nematic phase is characterized by a three-dimensional orientational order, as opposed to the conventional uniaxial nematic phase displaying a one-dimensional orientational order only. Sometimes, molecules with sufficient deviation from axial symmetry—which had been identified as biaxial nematics in optical studies[2]—turned out to be uniaxial when restudied by other techniques.[3] This indicates that not only the synthetic effort for the design of molecules with the desired shape to form a biaxial nematic phase[4] but also the search for an experimental method to unambiguously prove this biaxiality were greatly stimulated by Freiser's prediction. Apart from a ternary lyotropic system investigated by Yu and Saupe,[5] an accepted experimental proof for a biaxial nematic phase in a thermotropic liquid crystal (LC) remained missing for over 3 decades.

Already in 1973 Alben published his calculations based on a mean-field lattice model,[6] which indicated that a biaxial nematic phase could also be obtained by mixing suitable platelike and rodlike molecules. Although the concept was later found to be flawed by the potential thermodynamic instability of such mixtures,[7] it inspired many experimentalists to find miscible rod−disk systems or to link disks and rods chemically.[8] In 2003, Mehl and Kouwer published a miscibility study of a combined rod−disk mesogen that showed no miscibility gap with either of the pure components.[9] In DSC studies of discrete mixtures of the rod−disk mesogen and the pure disk they found a minimum in the transition enthalpy when approaching the minimum nematic to isotropic transition temperature. As this is typical for the occurrence of a biaxial nematic phase, and since the authors had also found an additional second-order phase transition below the nematic to isotropic transition for the mixture with this composition, they concluded that this was a biaxial nematic phase.

A first strong hint toward a biaxial nematic phase in an LC polymer was published already in the early 1990s by Leube and Finkelmann,[10] and we could detect phase biaxiality in a similar polymer by means of deuterium NMR in 2004.[11] In these polymeric systems the lateral attachment of the book-shaped mesogen with the polymer backbone is successful in hindering the rotation of the mesogen about its molecular long axis and thus supporting the formation of a biaxial nematic phase. In the same year, two papers on phase biaxiality in banana-shaped molecules were published. Madsen, Samulski, and co-workers found phase biaxiality with polarization microscopy and conoscopy on one hand, while obtaining less ambiguous evidence by means of deuterium NMR spectroscopy on the other hand.[12] Kumar and co-workers used X-ray diffraction measurements as the experimental method of choice.[13] The fact that the angle between the two mesogenic arms in theses systems is 140° and thus far outside the range for which a biaxial nematic phase has been predicted[14] indicates an important influence of the dipole moment. Finally, Merkel et al. published an infrared absorbance study on LC organo-siloxane tetrapodes in which they observed a weak first-order transition from an isotropic to a uniaxial nematic phase, followed by a second-order transition to a biaxial nematic phase.[15] This was nicely corroborated by recent ^{2}H NMR investigations,[16] which revealed similarities to our LC polymer in that the partial immobilization of the

* Present address: Martin-Luther-Universität Halle-Wittenberg, Fachbereich Physik, Friedemann-Bach Platz 6, D-06108 Halle/Saale, Germany. E-mail: kay.saalwaechter@physik.uni-halle.de.

10.1021/jp0605348 CCC: $33.50
Published on Web 07/25/2006

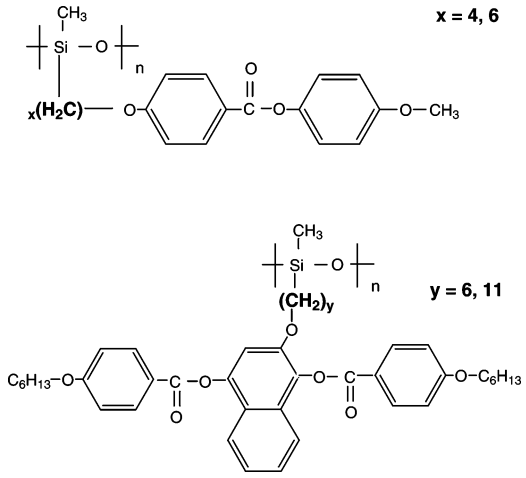

Figure 1. Chemical structure of the different types of investigated polymers: end-on polymer (top), side-on polymer (bottom).

mesogen via its attachment to a larger moiety might be a critical factor in stabilizing the biaxial phase in certain cases.

In our preceding publication[11] we could show that a side-on liquid crystalline side-chain polymer formed a biaxial nematic phase at low temperatures by using orientation-dependent deuterium NMR experiments. In contrast to that, an investigated end-on polymer showed exclusively uniaxial behavior in the whole range of the nematic phase. Here we expand our investigations to side-chain polymers of different chemical constitutions as well as to polymer mixtures, to evaluate different parameters that bias the formation of a biaxial nematic phase and gain a more general picture of phase biaxiality in nematic LC polymers.

Experimental Section

Samples. The investigated samples are two different side-chain polymers consisting of a polysiloxane backbone[17] with the mesogens terminally attached[18] via a flexible spacer of 4 and 6 carbon atoms (*end-on 4* and *end-on 6*, respectively) as well as two side-on polymers[19] with spacer lengths 11 and 6 in mixtures with low molar mass LCs (termed *side-on 11 mix* and *side-on 6 mix*, respectively). Mixing mainly served to reduce the glass transition temperatures and thus provide a possibility to study its influence. As a comparison, results from the undiluted *side-on 11* polymer from the previous publication are given.

Details about the synthetic concepts can be found in the corresponding references, and the chemical structures of the two different polymer types are given in Figure 1. Generally, the polymers are obtained by grafting of the mesogenic side groups to a chain-extended poly(methyl hydrogen siloxane) precursor polymer (DP $\approx$ 260). The related substantial change in composition is the reason that direct comparisons between the monomeric mesogens and the final polymers are not immediately meaningful for this class of materials.

The side-on 11 mix sample was prepared by dissolving the polymer in benzene in the presence of 2% w/w 8CB (4-*n*-octyl-4′-cyanobiphenyl), followed by the evaporation of the solvent under high vacuum conditions. For the side-on 6 mixture, an amount of 10% w/w 4-octyloxyl-4′-hexyloxylbenzoate was added instead for miscibility reasons. In all samples 2% w/w of perdeuterated hexamethylbenzene (HMB-d_{18}) were dissolved as a nuclear spin probe. Due to the restricted rotational diffusion of the probe within the LC phase, coupled with spatial averaging over the length scale of the translational diffusion length, it

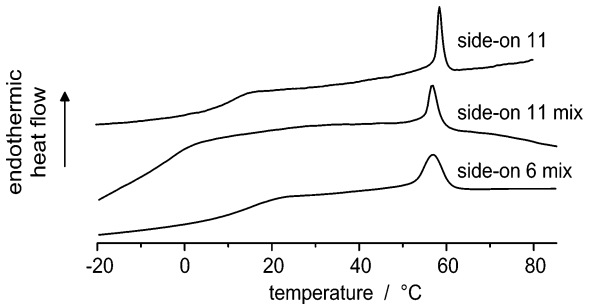

Figure 2. Exemplary DSC traces (heating rate 25 K/min) for three of the samples.

TABLE 1: Transition Temperatures (K) and Average Transition Enthalpies (J/g) for the Different Investigated Samples

sample	T_g	T_{SN}	T_{NI}	ΔH_{NI}
side-on 11	279		329	2.5
side-on 11 mix	~260		326	3.4
side-on 6 mix	280		324	3.3
end-on 4	280		363	2.4
end-on 6	274	317	374	2.8

reveals the symmetry of the particular LC phase. In addition to the well-known limitation that the nematic order parameter of the mesophase cannot easily be derived from deuterium splittings of a spin probe, very recent work of Luckhurst and coworkers even indicated that different probes may have a different sensitivity to the actual phase biaxiality, as found in experiments on a biaxial soft crystal phase.[20] Therefore, results from probe experiments must be considered *qualitative*; the actual phase biaxiality could be higher than the value obtained from the spin probe.

Phase Behavior. The transition temperatures and enthalpies of the different samples were measured by differential scanning calorimetry (DSC). All investigated samples display a nematic phase above the glass transition, except for the end-on 6 polymer, which forms an additional smectic below the nematic phase. Three exemplary DSC traces for the side-on 11, side-on 11 mix, and the side-on 6 mix samples with heating rates of 25 K/min are given in Figure 2. The transition temperatures were obtained by extrapolating to heating rates of 0 K/min.

The transition temperatures in K as well as the average enthalpies for the nematic to isotropic transition in units of J/g for all samples are listed in Table 1. As a comparison the data for the original side-on 11 polymer are included. The transition temperatures T_{NI} as measured by NMR experiments were deviating by less than 3 K. At the transition temperatures obtained by DSC the samples were, according to the NMR spectra, usually still in the two-phase region. For the following calculations and plots, the T_{NI} values obtained by NMR were used.

Sample Preparation and Setup. The samples were prepared in standard NMR glass tubes with an inner diameter of 4.5 mm between silicon spacers coated with Teflon on the inner side facing the sample. The NMR probe used for measurements under various angles was a standard static Bruker double resonance probe modified with a goniometer in the following way: An axle was inserted into the probe reaching from the sample holder down to a rotary magnet attached at the bottom of the probe, and the sample was fixed tightly inside an O-ring within a cog wheel, which in turn was joined with a second cog wheel driven by the axle. Using trigger pulses from the NMR console, the rotary magnet allows for fast sample rotations up to 90° in less than 150 ms. The accuracy of the angle setting

was checked by angle-dependent measurements of the quadrupolar splitting in the oriented smectic phase of α-deuterated 8-CB and was found to be on the order of 1°. As the second Legendre polynomial is flat in the canonical orientations, the influence of this error on the results reported herein is negligible.

NMR Techniques. The NMR measurements were performed on a Bruker Avance 500 solid-state NMR spectrometer with a magnetic field strength of $B_0 = 11.7$ T and a corresponding deuterium resonance frequency of 76.773 Hz. The pulse sequence used for the determination of the quadrupolar splitting of an aligned sample was a regular solid echo acquired at the top of the echo under exact on-resonance condition. The dwell time was 2.5 μs, the $\pi/2$ pulse length around 4 μs, the pulse spacing 43 μs, and the recycle delay 0.5 s. Depending on the sample and the actual temperature, a number of 256 up to 2048 transients were averaged for sufficient signal-to-noise. As in the work of Yu and Saupe we derive the biaxiality parameter of the different samples from measurements of the quadrupolar splitting, $\Delta\nu_q(\beta)$, at different angles β between the main director of an annealed monodomain and the static magnetic field

$$\nu_q = \nu_0 \pm \frac{3}{4} q_{zz} \frac{1}{2} (3\cos^2\beta - 1 - \eta \sin^2\beta) \qquad (1)$$

where ν_0 is the deuterium resonance frequency, q_{zz} is the z principle component of the quadrupole tensor, and η is the biaxiality parameter defined as

$$\eta = \frac{q_{yy} - q_{xx}}{q_{zz}} \qquad (2)$$

With experimental splittings of a sample with the main director oriented along the magnetic field and perpendicular to it, the biaxiality parameter is easily calculated from the ratio according to

$$\eta = 1 + \frac{2q_{yy}}{q_{zz}} = 1 - \frac{2|\Delta\nu_q(90°)|}{|\Delta\nu_q(0°)|}. \qquad (3)$$

Equation 3 holds because the quadrupole tensor is traceless; i.e., with the knowledge of merely two components of the tensor, η can be calculated. We call the determination of the biaxiality parameter according to this procedure the tilt experiment. Under the assumption of exponential relaxation by an apparent T_2*, the spectra were fitted with two Lorentzians of equal amplitude separated by $\Delta\nu_q$. A narrow peak associated with a small amount of isotropically mobile HMB in phase-separated impurities that appeared in the central region of the spectra was either fitted by a third Lorentzian (see Figure 6 below) or excluded from the fits, which gave virtually identical results. For the calculation of the biaxiality parameter at a certain temperature, both the 0° and the 90° spectra were acquired several times in order to obtain error intervals based on average reproducibility and reliability of line shape fittings. The standard deviation for η was in all cases on the order of ± 0.01.

To avoid inaccuracies in the determination of the 90° splitting due to director relaxation during the measurements, we used the technique introduced by Zhou and Frydman,[21] where the sample is positioned along the desired angle β for the actual pulse sequence and acquisition only (about 200 ms). For the considerably longer recycle delay, which is needed for the spins to return to their thermal equilibrium, the monodomain sample is rotated back to its equilibrium orientation along the magnetic field. For the creation of a three-dimensional monodomain, the sample should in principle undergo repeated rotation followed by the relaxation of the major director (q_{zz}), so as to force the minor directors (q_{xx} and q_{yy}) into a minimal energy configuration. In our case it was not possible to experimentally verify a planar polydomain of q_{xx} and q_{yy} when simply tilting the sample about an angle of 90°. That means that a tilting-relaxation procedure to produce a monodomain was not necessary. From this observation we draw the important conclusion that the alignment of the secondary director is probably rather fast, i.e., on the order of tens of milliseconds. It may either occur via a magnetic torque in the $q_{xx}-q_{yy}$ plane combined with a low local viscosity for rotations around q_{zz} or due to accumulating weak director relaxation/viscous friction effects during a small initial fraction of the few hundred flip experiments that make up the total number of recorded transients.

For the determination of the relaxation times of the major director, the samples were rotated about an angle of 48°, followed by the acquisition of consecutive spectra. For each spectrum the quadrupolar splitting was determined, from which the actual average angle between the main director and the magnetic field over that interval in time could be calculated in turn. Plotting the tangent of that particular angle versus the corresponding time yielded the director relaxation time τ according to[22]

$$\tan[\beta(t)] = \tan[\beta(t=0)] \exp\left[-\frac{t}{\tau}\right] \qquad (4)$$

The quality of these fits was good, and an example can be inspected in Figure 1 of our previous paper.[11]

Transverse relaxation times (T_2) were measured with a solid-echo pulse sequence with stepwise increasing delays after the first pulse and before the signal acquisition. The relaxation times were obtained by plotting the signal intensity versus the corresponding time using a monoexponential fit. From the T_2 values theoretical line widths (full width at half-maximum, fwhm) were calculated according to

$$\text{fwhm} = 1/(\pi T_2) \qquad (5)$$

which is based on the assumption of a purely homogeneous Lorentzian line and negligible linear (chemical shift and susceptibility) contributions. A comparison between these calculated values with the actual line widths obtained from the Lorentzian fits provides a first hint toward an inhomogeneous contribution to the line widths. Such a contribution could be caused by a certain director orientation distribution that is stable on the time scale of the NMR experiment and possibly also by a planar polydomain of q_{xx} and q_{yy} in the case of a flipped sample. Note that the latter phenomenon would not lead to the erroneous observation of an apparent η, since the frequency distribution would be symmetric around the splitting corresponding to $-q_{zz}/2$, at least for small η where the two parts of the doublet do not overlap. As any other type of underlying inhomogeneous broadening might interfere with a precise measurement of the quadrupolar splittings and thus with the determination of the biaxiality parameter, these inhomogeneous contributions to the line shape were confirmed by two-dimensional Hahn-echo correlation experiments.[23]

The pulse sequence for this experiment is indicated in Figure 3. The Hahn echo in the t_1-dimension (indirect dimension) serves to refocus first-order contributions, such as susceptibility effects (caused by, e.g., an air bubble in the sample). To obtain a purely absorptive two-dimensional spectrum, we acquired only a cosine dataset, which was possible because the two peaks in the observed doublet are well separated. The use of this cosine

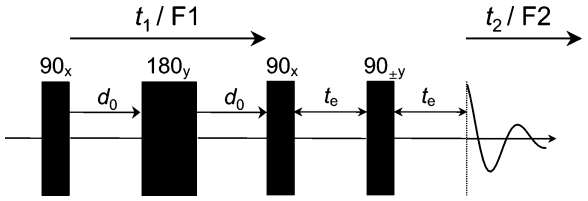

Figure 3. Pulse sequence for the two-dimensional correlation experiment.

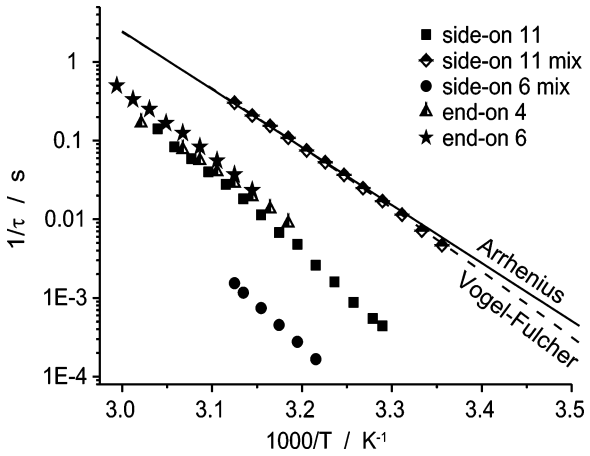

Figure 4. Arrhenius behavior of the director relaxation times of the different samples. Side-on 11 (squares), side-on 11 mix (diamonds), side-on 6 mix (circles), end-on 4 (triangles), and end-on 6 (stars). Exemplary Arrhenius and Vogel−Fulcher fits are included for the side-on 11 mix sample.

modulation leads to the appearance of quadrupolar splitting along both the diagonal and the antidiagonal, as will be seen in the next section.

On one hand, a comparison between projections onto the F_1 and F_2 frequency dimensions can provide information about potential errors due to susceptibility effects mentioned above, since these are not being refocused during t_2. On the other hand, a quasi-static director distribution results in a pronounced diagonality of the peaks in the two-dimensional spectrum. The difference between the line width of a peak along the diagonal and its width parallel to the antidiagonal represents a measure for the inhomogeneous broadening, i.e., director distribution effects. Both the T_2 and the two-dimensional (2D) experiments were conducted on samples oriented along the magnetic field as well as in the 90° tilted configuration. The results from the 2D experiments form the basis for rather conservatively calculated error intervals for the biaxiality parameter η, as discussed below.

Results and Discussion

In this section we discuss the results of our measurements for the different polymer systems. In the first part we present the results for the director relaxation experiments, and in the second part the temperature-dependent quadrupolar splittings for the different systems are given. These splittings carry information on the order parameter as well as the coupling of the spin probe to the liquid-crystalline phase. Then, we discuss the influence of disorder and dynamic processes on the experimental time scale as possible sources of artifacts. Finally the onset of detectable phase biaxiality in the different samples is compared in relation to the isotropic−nematic and glass transition temperatures.

Director Relaxation Measurements. Director relaxation measurements have been conducted on each sample for several

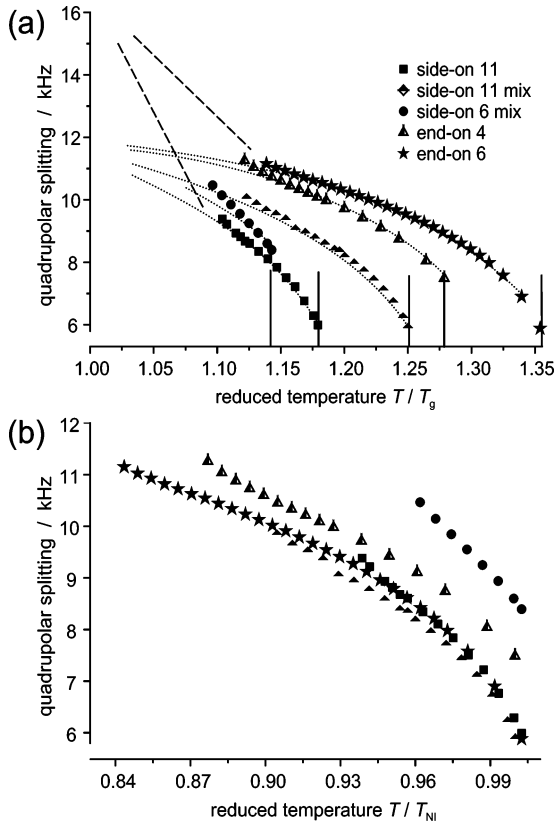

Figure 5. Quadrupolar splittings for the different systems in samples oriented along the magnetic field as a function of T/T_g (a) and as a function of T/T_{NI} (b). The symbols correspond to those used in Figure 4, and in (a) the vertical lines indicate T_{NI} of each sample. The dashed and dotted lines are just guides to the eye.

temperatures within the LC phase. The upper limits are set by T_{NI}, and the lower limits by excessive line broadening upon approaching the glass transition or, in case of the end-on 6 polymer, by T_{SN}. Within the accessible temperature range all polymers show a nearly linear dependence of the logarithm of the rate constants ($1/\tau$) on the reciprocal temperature, as can be seen in Figure 4. This is typical for an activated process following an Arrhenius behavior.

For the sake of clarity an exemplary Arrhenius fit for one sample only is shown in Figure 4. However, the activation energy obtained from that fit (150 kJ/mol) is unrealistically high, as is the frequency factor with 6×10^{23} s^{-1}. (For the other systems the activation energy is between 150 and 200 kJ/mol, and the frequency factor in the range of $10^{22}-10^{30}$ s^{-1}.) This is due to the rotational viscosity associated with the director relaxation time being strongly coupled to the dynamics of the polymer chain. Upon approaching T_g, the slow-down of the chain modes therefore leads to a downturn of ln k. This is typical for polymers that usually do not follow an Arrhenius behavior but display a Vogel−Fulcher (VF) dependence[24]

$$\ln(1/\tau) = \ln A - \frac{E_a}{R(T - T_v)} \qquad (6)$$

where T_v is the Vogel temperature, which is located roughly 51 K below the glass transition.[25] However, this divergence is hardly visible in our data, since the accessible temperature range is too narrow for reasons mentioned above. This can also be seen in an exemplary Vogel−Fulcher fit for the side-on mix polymer in Figure 4.

Quadrupolar Splittings and Order Parameters. Quadrupolar spectra were acquired for several temperatures within the

liquid-crystalline phases of all the different systems using a the standard solid-echo sequence. The quadrupolar splittings as obtained from Lorentzian fits of these spectra as a function of T/T_g (a) and T/T_{NI} (b) are presented in Figure 5.

The dotted lines in Figure 5a are guides to the eye, representing the typical temperature dependence of the order parameter (the order parameter is directly proportional to the quadrupolar splitting). At lower temperatures deviations from the expected trend in the form of an upturn can be recognized. Due to the slowdown of the probe diffusion upon approaching the glass transition, the splitting can increase significantly faster than expected, indicated by the dashed lines. This indicates one of the limits of the probe method: its rotational diffusion must be in the fast limit in order to properly reflect the mesophase symmetry (i.e., fast compared to the inverse intra-CD_3 quadrupole coupling constants). Otherwise, increasingly strong inhomogeneous contributions to the line shape in analogy to a powder spectrum arise and ultimately challenge the determination of η.

To gain some limited insight into the nematic order parameter and the coupling of the probe to the mesophase order, we assume that the most likely orientation of the HMB ring in a nematic phase composed of calamitic aromatic mesogens is the one with the ring normal at 90° to the director (i.e., all benzene rings are coplanar). Assuming a fast-limit (diffusional) averaging of the ring normal in the transverse plane (that produces uniaxial symmetry with respect to the director and contributes a factor of 2 reduction), a splitting of about 16 kHz would be expected, since the combined effect of faster methyl rotation and rotation around the C_6 axis, that are both in the fast limit even in crystalline HMB at ambient temperature, produce a Pake spectrum with 32 kHz width.[26] The latter was also checked experimentally. A 16 kHz splitting could thus be expected for the case of perfect coupling to the mesophase symmetry and $S = 1$. The fact that the splittings extrapolate to roughly 11 kHz without the T_g effect, corresponding to an apparent order parameter of about 0.7, which is in the typical range for nematic ordering well below T_{NI}, indicates that the coupling constant of the diffusing spin probe to the director field is probably on the order of unity.

An exception is represented by the side-on 6 mix sample, for which the quadrupolar splitting exhibits some deviation from the general trend. Figure 5b shows the quadrupolar splittings for the different systems as a function of T/T_{NI}. The temperature-dependent behavior is very similar for the different systems, again with the exception of the side-on 6 mix. This polymer shows an almost linear increase of the splitting as a function of T/T_{NI}. Both polymers with the shorter spacers (end-on 4 and side-on 6 mix) display comparably larger quadrupolar splittings than the ones with the longer spacers. A possible reason for this is obviously the closer relative proximity of T_g, thus the higher viscosity of these systems as compared to the ones with the longer spacers. In this case, not only the spatial averaging but also the restricted rotational diffusion slows down, thus the probe cannot reorient quickly enough to properly pick up the LC domain ordering, as discussed above.

Influence of Disorder and Intermediate Motions The tilt experiment for the determination of the biaxiality parameter was conducted on all different polymer systems for several temperatures within the LC phase. Multiple measurements were done for each temperature and both angles. Figure 6 shows experimental results for all samples for which phase biaxiality was observed, which, surprisingly, was also the case for the end-on 4 sample. The biaxiality will be discussed further below, and we first focus on possible sources of error.

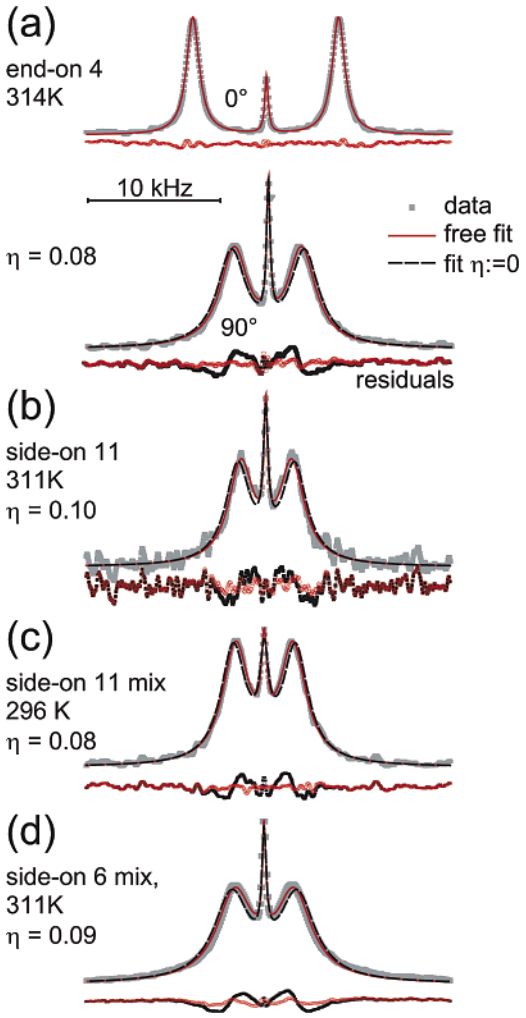

Figure 6. Results of tilt experiments conducted on the various samples. In (a), a 0° spectrum (top) is compared with a 90° spectrum (bottom) for the end-on 4 sample. In (b−d), only 90° spectra are shown, along with free Lorentzian fits, fits imposing $\eta := 0$ (half the 0° splitting), and the respective residuals. The small, isotropic center peak from HMB in impurities is accounted for by a third Lorentzian.

In all cases, good fits of the data were provided by Lorentzian doublets (plus another narrow Lorentzian for the HMB in impurities), as can be judged from the residuals in Figure 6. This represents a first indication that the line width is in all cases dominated by (exponential) relaxation processes rather than a frequency distribution. For the 90° spectra, we also show fits and residuals for the case where the splittings were fixed at half the 0° values, and these fits are clearly not satisfactory.

Relaxation-induced homogeneous line broadening is in most cases Lorentzian and, more importantly, always symmetric for a given isochromate. It is therefore not expected to interfere with a precise determination of the splitting, at least for cases where η is small. As is indicated by the residuals in Figure 6d (which was acquired with considerably more scans) there are however small deviations from the Lorentzian shape, which are explained by weak inhomogeneous contributions to the line shape. In such a case, the fitted value can be an essentially uncontrolled average, and the degree of frequency distribution needs to be determined in order to obtain a proper estimate of the possible errors inherent to our approach to asses the biaxiality.

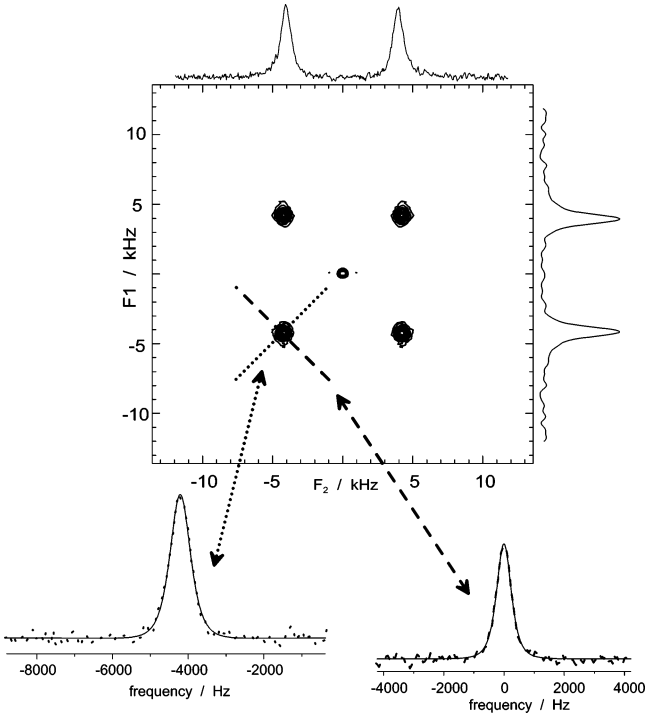

Figure 7. Two-dimensional ^{2}H correlation spectrum of the side-on 11 polymer at 316 K. Projections onto the direct and indirect dimension are given on top and on the right-hand side of the spectrum. Projections onto the diagonal and parallel to the antidiagonal are shown at the bottom.

To determine the degree of inhomogeneous broadening, we performed, in addition to solid-echo T_2 relaxation measurements, two-dimensional ^{2}H correlation experiments as introduced in the Experimental Section. Such a 2D spectrum is shown in Figure 7 for the side-on 11 polymer at 316 K for the nontilted case. First-order contributions to the broadening (e.g., susceptibility effects) were found to be negligible by comparing projections onto the direct and the indirect dimensions, which were deviating neither in the line width nor in the splitting by more than 1%.

The degree of inhomogeneous broadening, which might arise from a director distribution that is stable on the experimental time scale and extends over length scales that exceed the probe diffusion length, or by contributions from a planar powder as a result of incomplete monodomain ordering of q_{xx} and q_{yy}, was found to be small by comparing the line width of projections onto the diagonal (940 Hz) and parallel to the antidiagonal (820 Hz), which differ by 120 Hz only. This value is in very good agreement with the estimation of inhomogeneous broadening obtained from T_2 measurements and the comparison with the actual line width. For the side-on 11 polymer at 316 K a T_2 value of 406 μs was measured, corresponding to a line width of 784 Hz according to eq 5 for the case of a purely homogeneously broadened Lorentzian. The average measured line width exceeded this value by 124 Hz, which is consistent with the result from the 2D spectrum. The same measurements were conducted for a tilt angle of 90°, where an inhomogeneous contribution of 75 Hz was found. The data for all different systems are summarized in Table 2. In most cases the results from the one-dimensional measurements agreed quite well with those obtained from the two-dimensional spectra. Deviations at low temperatures and/or tilt angles of 90° are probably due to rather low signal-to-noise ratios.

To take into account these contributions when calculating the biaxiality parameter, we assume that the 0° and the 90° splitting can only be determined within these diagonal/antidiagonal intervals of 120 and 75 Hz, respectively. The difference between the η values resulting from the smallest 90° splitting (lower end of the 90° interval) and the largest 0° splitting (upper end of the 0° interval) as well as the largest 90° and the smallest 0° splitting, respectively, are taken as rather conservative worst-case errors for this particular temperature. Note again that additional uncertainties arise as T_g is approached, where the probe diffusion, in particular the in-plane averaging of the ring normal, slows down and may lead to even larger distributions, in particular in the 90° orientation. For the temperatures collected in Table 2, there is no indication for this effect, as the inhomogeneous contributions found at 90° are always significantly smaller than those at 0°. With the same argument, significant contributions from a planar polydomain can also be excluded.

TABLE 2: Summarized Data for the Line Broadening in the Different Investigated Systems at Selected Temperatures

				fwhm/Hz		inhomogeneous broadening/Hz	
	T (K)	angle/deg	T_2/μs	eq 5	exptl	fwhm difference	2D
side-on 11	316	0	406	784	908	124	120
		90	218	1460	1510	50	75
	311	0	271	1175	1342	167	220
		90	122	2609	2707	98	90
side-on 11 mix	311	0	1150	277	384	107	100
		90					50
	302	0	610	522	670	148	220
		90					90
side-on 6 mix	319	0	520	610	850	240	250
		90	290	1100	1150	50	100
	311	0	305	1040	1310	270	270
		90	135	2360	2490	130	150
end-on 4	332	0	1267	251	410	159	200
		90	1320	241	310	69	
	316	0	423	753	931	178	180
		90	170	1872	1960	88	

Whether the inhomogeneous contribution really originates from the quasi-static part of an otherwise slowly fluctuating director (i.e., from the slow end of a wide and spatially heterogeneous director fluctuation time distribution that is coupled to T_g) or if it is caused by the spin probe molecule sensing wall-induced domain heterogeneity within the sample cannot be answered on the basis of these data. Notably, the inhomogeneous contribution is about half in the 90° configuration in all cases, which, however, is expected for both scenarios.

Another important issue when considering possible artifacts in determining η is whether the splittings themselves are, apart from the substantial but well-defined homogeneous broadening, subject to an orientation-dependent dynamic frequency shift, that could ultimately mimic a nonzero η. Line broadening in mobile LC phases is commonly discussed in terms of relaxation induced by intermediate time scale director fluctuations. In our case, the relaxation could be either due to fluctuations of the director itself or, when diffusion is the faster process, due to the probe picking up different orientations on its way.

Both scenarios can ultimately be described within the same model framework of a rotational diffusion process of the local symmetry axis of the quadrupole tensor. Frezzato et al. have recently published a relaxation theory for director fluctuations in oriented LC systems,[27,28] and from their work we infer that such a dynamic frequency shift indeed exists, yet that it (rather intuitively) becomes significant only in the fast-motion domain, i.e., when the director fluctuations become much faster than the inverse splitting. This effect should therefore increase with

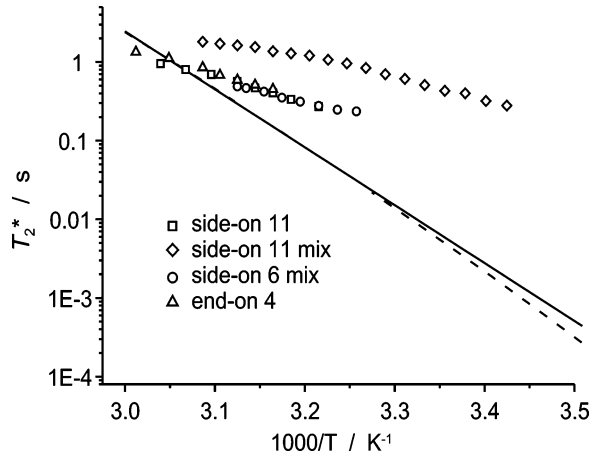

Figure 8. Arrhenius plot for T_2*, calculated from the fitted fwhm using eq 5, of the different samples measured in the 0° orientation. The data are plotted on the same scale as in Figure 4, and the lines are the trends for the inverse director relaxation times $1/\tau$ of the side-on 11 mix sample shown in that figure.

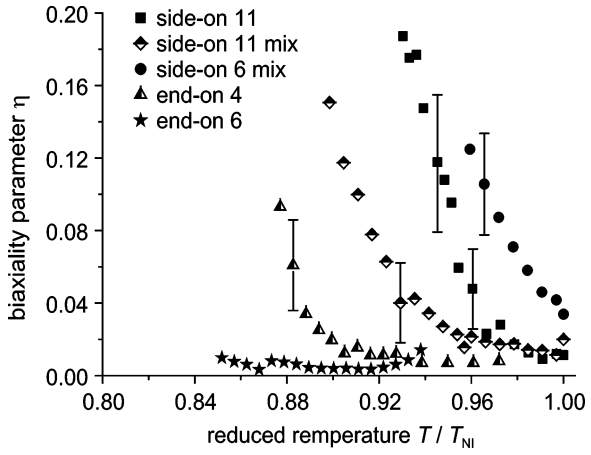

Figure 9. Temperature dependence of the biaxiality parameter for the different investigated polymer systems.

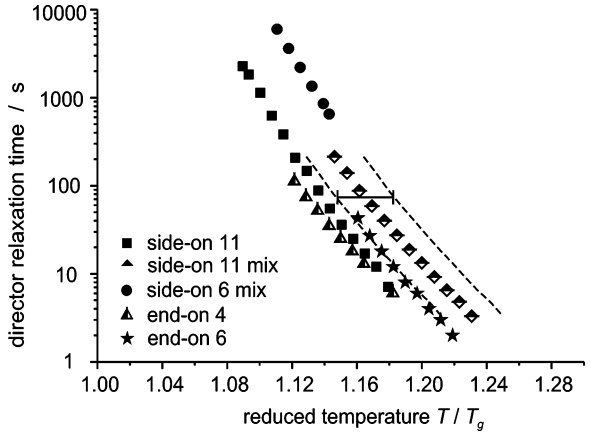

Figure 10. Semilogarithmic plot of the director relaxation times of the different samples. The dashed lines indicate the effect of a relatively wide error interval for the glass transition of the side-on 11 mix sample.

increasing temperature, whereas biaxiality increases with *decreasing* temperature. We can therefore exclude a dynamic frequency shift as a possible source of artifact.

To decide whether the line broadening is dominated by the time scale of diffusion or actual director dynamics, we plot the apparent T_2* relaxation times (calculated from the inverse line widths, neglecting the weak peak heterogeneity) vs inverse temperature in Figure 8 and compare it to the macroscopic director relaxation rates $1/\tau$ shown in Figure 4. Since the T_2 process approaches the fast limit upon raising the temperature (narrower lines at higher T), T_2 should in this region be roughly proportional to the inverse correlation time of the associated process. In this case, a comparison with the macroscopic director relaxation, which is also coupled to the (Leslie rotational) viscosity of the sample, should reveal if probe diffusion over differently oriented domains is the cause of the T_2 process.

Figure 8 shows that this is not the case—the apparent activation energy of the T_2 process is much lower than that of the viscosity-dominated director relaxation, indicating different molecular origins, and we conclude that intermediate fluctuations of the major director itself, which are of a more cooperative nature, are responsible. This interpretation is of course based on the assumption that the viscosity associated with the probe diffusion and the rotational viscosity probed by the director relaxation experiments are governed by the same VF relationship. These aspects certainly deserve more attention in future work on polymeric LCs.

Phase Biaxiality. Figure 9 displays the average biaxiality parameters as a function of the reduced temperature T/T_{NI} for the different investigated systems. For the sake of clarity the error intervals based on the statistical errors from multiple measurements, which vary between ± 0.005 and ± 0.015 are omitted in the graph. Exemplary error intervals as obtained from the 2D experiments are included for each polymer system, except for the end-on 6 polymer, for which no 2D experiments were conducted in the 90° configuration.

The results of the investigations of the end-on polymers, where the mesogenic units are terminally connected to the polymer backbone, show that a long spacer enables a decoupling of the LC and the polymer. The end-on 6 polymer displays a uniaxial behavior over the entire region of the nematic phase and is in this sense resembling a low molar mass LC. In contrast, the end-on 4 polymer shows a biaxial nematic phase at low temperatures. This proves the important influence of the spacer length between the mesogenic unit and the polymer backbone. The reduction of the spacer length from six to four carbon atoms induces an alteration of the properties away from those of a low molar mass LCs, indicating that a complete decoupling between the mesogen and the polymer cannot be accomplished.

Even though the molecular biaxiality is clearly less pronounced in the end-on mesogen as compared to the side-on cases, the formation of a biaxial nematic phase is clearly observed. A reduction of the spacer length from 11 to 6 carbon atoms for the side-on polymer results in an increase of the biaxiality parameter at comparably reduced temperatures. For the side-on 6 polymer the existence of a uniaxial nematic phase is not apparent. Generally, given the limited accuracy of the data, we refrain from reporting uniaxial to biaxial transition temperatures. Figure 9 merely indicates that the transitions are of second order, in agreement with the similar results on organosiloxane tetrapodes.[16]

The addition of a low molar mass LC, which induces a shift of the glass transition to lower temperatures, results in a decreased temperature-dependence of the biaxiality parameter. The onset of increasing biaxiality parameters is shifted toward lower reduced temperatures. The importance of polymer dynamics for the formation of a biaxial nematic phase is demonstrated in more detail in the following.

To emphasize again the significance of the glass transition temperature, the director relaxation times for the different systems are plotted as a function of T/T_g in Figure 10 on a semilogarithmic scale. The dotted lines along side the data for

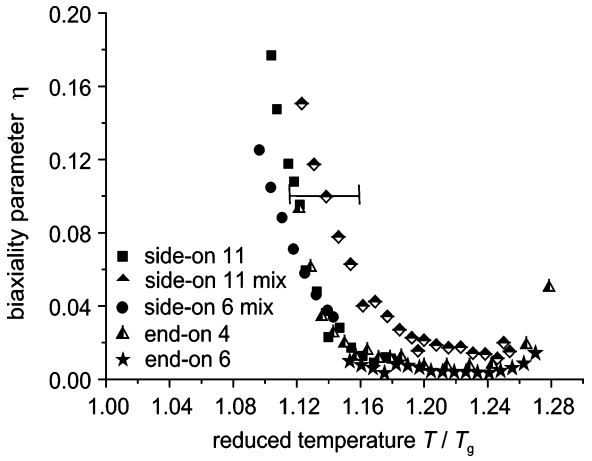

Figure 11. Temperature-dependence of the biaxiality parameter for the different investigated polymer systems, now plotted vs a different reduced temperature T/T_g. The large error interval for the side-on 11 mix sample again indicates the ambiguity in assigning a glass transition temperature.

the side-on 11 mix sample are a guide to the eye and indicate the rather wide error interval ($\pm$4 K) that originates from the difficulty to assign the glass transition temperature T_g, which is rather smeared out in the DSC scans of this sample. Taking this into account, all investigated systems show a very similar behavior with the exception of the side-on 6 mix sample. The director relaxation times for this system are substantially larger than for the other systems at comparable temperatures T/T_g.

In Figure 11 the biaxiality parameters for the different systems are plotted as a function of T/T_g. Again, when taking into account the relatively wide error interval for the glass transition temperature of the side-on 11 mix system, the temperature-dependent behavior is now very similar for all investigated systems. The formation of a biaxial nematic phase occurs upon approaching the glass transition temperature at roughly $T/T_g \sim 1.16$. This clearly demonstrates the decisive role of the glass transition and thus the importance of polymer dynamics for the stabilization of the biaxial nematic phase. Note that the (apparent) upturn of η toward higher temperatures that is now well visible for some samples is due to the onset of director reorientation during its short residence time at 90°. The effect is not important at lower temperatures, where the viscosity decreases.

In this graph, a critical issue arises: in the temperature region where a biaxial nematic phase is observed, the only uniaxial end-on 6 polymer forms a smectic phase, which prevented studies at temperatures which are comparably close to T_g. We therefore still lack the demonstration of a uniaxial phase at such lower temperatures. For a final confirmation that end-on polymers with long spacers do not form biaxial nematic phases, experiments conducted on an additional polymer that does not exhibit a low-temperature smectic phase will be necessary. The suppression of a smectic phase is usually achieved by the introduction of lateral substituents,[29] which however requires a totally different (asymmetric) synthetic route that was beyond the scope of the present work.

However, it is worth pointing out that *qualitative differences* between end-on polymers with spacers of lengths 4 and 6 have been observed before in earlier studies of cholesteric systems, where the helical twisting power was found to strongly increase with decreasing spacer length.[30,31] In the framework of the theory of Goossens,[32] this effect can be explained by an order parameter that describes the hindered rotation of the mesogens about their molecular long axis. In how far these observations are directly or indirectly related to the stabilization of phase biaxiality in such systems must be the subject of future theoretical work on the influence of spacers, the motivation for which we hope to have provided here.

Besides that, recent investigations on cholesteric LC side-on polymers by Ogawa et al.[19] are consistent with our findings of biaxial nematic phases in side-on LC polymers: they found that mixtures with more than 60 mol % of a cholesteric copolymer corresponding to the side-on 6 polymer did not exhibit a conventional fingerprint texture typical for cholesteric liquid crystals. In this case the phase biaxiality, that we here observe directly, can be made responsible for disturbing the smooth optical periodicity of the cholesteric phase structure.

Conclusion

With our experiments we could show that even end-on polymers are capable of forming biaxial nematic phases. This is the case if the spacer between the polymer backbone and the mesogenic unit is short and therefore does not allow for an unhindered rotation about the molecular long axis. The addition of a low molar mass LC is lowering the glass transition temperature in a similar way as the transition from the uniaxial to the biaxial nematic phase. By plotting the biaxiality parameter as a function of T/T_g for the different investigated systems, we found that the transition to the biaxial nematic phase occurs at roughly the same value of T/T_g for the different polymers. This proves the decisive role of the polymer dynamics for the formation of a biaxial nematic phase.

Besides the desired synthesis and analysis of an end-on polymer with a long spacer that does not display a smectic phase at low temperatures and should not exhibit phase biaxiality close to T_g, our future work is focused on diffusion measurements of the nuclear spin probe HMB in a biaxial nematic phase in order to investigate in more detail the length scales and the anisotropy of spatial averaging in polymeric LC systems and the relation to the strong increase of the overall viscosity upon approaching T_g. The overall goal will be the determination of the diffusion tensor for which a new setup has to be implemented in order to access diffusion coefficients in a three-dimensionally oriented monodomain in all three directions in space.

Acknowledgment. We acknowledge financial support from the Deutsche Forschungsgesellschaft (Grant Fi 279/14) and the Fonds der Chemischen Industrie.

References and Notes

(1) Freiser, M. J. *Phys. Rev. Lett.* **1970**, *24*, 1041−1043.
(2) Malthête, J.; Thin, N. H.; Levelut, A. M. *J. Chem. Soc., Chem. Commun.* **1986**, 1548−1549.
(3) Hughes, J. R.; Kothe, G.; Luckhurst, G. R.; Malthête, J.; Neubert, M. E.; Shenouda, I.; Timini, B. A.; Tittelbach, M. *J. Chem. Phys.* **1997**, *107*, 9252−9263.
(4) Straley, J. P. *Phys. Rev. A* **1974**, *10*, 1881−1887.
(5) Yu, L. J.; Saupe, A. *Phys. Rev. Lett.* **1980**, *45*, 1000−1003.
(6) Alben, R. *J. Chem. Phys.* **1973**, *59*, 4299−4304.
(7) Sharma, S. R.; Palffy-Muhoray, P.; Bergersen, B.; Dunmur, D. A. *Phys. Rev. A* **1985**, *32*, 3752−3755.
(8) Hunt, J. J.; Date, R. W.; Timimi, B. A.; Luckhurst, G. R.; Bruce, D. W. *J. Am. Chem. Soc.* **2001**, *123*, 10115−10116.
(9) Kouwer, P. H. J.; Mehl, G. H. *J. Am. Chem. Soc.* **2003**, *125*, 11172−11173.
(10) Leube, H. F.; Finkelmann, H. *Makromol. Chem.* **1991**, *192*, 1317−1328.
(11) Severing, K.; Saalwächter, K. *Phys. Rev. Lett.* **2004**, *92*, 125501.
(12) Madsen, L. A.; Dingemans, T. J.; Nakata, M.; Samulski, E. T. *Phys. Rev. Lett.* **2004**, *92*, 145505.
(13) Acharya, B. R.; Primak, A.; Kumar, S. *Phys. Rev. Lett.* **2004**, *92*, 145506.
(14) Luckhurst, G. R. *Thin Solid Films* **2001**, *393*, 40−52.

(15) Merkel, K.; Kocot, A.; Vij, J. K.; Korlacki, R.; Mehl, G. H.; Meyer, T. *Phys. Rev. Lett.* **2004**, *93*, 237801.
(16) Figueirinhas, J. L.; Cruz, C.; Filip, D.; Feio, G.; Ribeiro, A. C.; Frère, Y.; Meyer, T.; Mehl, G. H. *Phys. Rev. Lett.* **2005**, *94*, 107802.
(17) Finkelmann, H.; Rehage, G. *Makromol. Chem. Rapid Commun.* **1980**, *1*, 31.
(18) Kniesel, S.; Cholesteric Liquid Crystalline Polymers. Dissertation, Universität Freiburg, 2005.
(19) Ogawa, H.; Stibal-Fischer, E.; Finkelmann, H. *Macromol. Chem. Phys.* **2004**, *205*, 593.
(20) Luckhurst, G. R. NMR Determination of the Symmetry of Liquid Crystal Phases. How Reliable are Spin Probes?, Paper presented at the 34. Arbeitstagung Flüssigkristalle, Freiburg, 2006.
(21) Zhou, M.; Frydman, V.; Frydman, L. *J. Am. Chem. Soc.* **1998**, *120*, 0, 2178−2179.
(22) Lesot, P.; Emsley, J. W.; Courtieu, J. *Liq. Cryst.* **1998**, *25*, 123−127.
(23) Schmidt-Rohr, K.; Spiess, H. W. *Multidimensional Solid-State NMR and Polymers*; Academic Press: London, 1994.
(24) Strobl, G. *The Physics of Polymers*; Springer-Verlag: Berlin, 1997.
(25) Williams, M. L.; Landel, R. F.; Ferry, J. D. *J. Am. Chem. Soc.* **1955**, *77*, 3701−3707.
(26) Schmidt, C.; Blümich, B.; Spiess, H. W. *J. Magn. Reson.* **1988**, *79*, 269−290.
(27) Frezzato, D.; Kothe, G.; Moro, G. J. *J. Phys. Chem. B* **2001**, *105*, 1281−1292.
(28) Frezzato, D.; Moro, G. J.; Kothe, G. *J. Chem. Phys.* **2003**, *119*, 6931−6945.
(29) Weissflog, W.; Demus, D. *Cryst. Res. Technol.* **1984**, *19*, 55.
(30) Ciferri, A.; Krigbaum, W. R.; Meyer, R. B. *Polymer Liquid Crystals*; Academic Press: New York, 1982.
(31) Finkelmann, H. *Philos. Trans. R. Soc. London, Ser. A* **1983**, *309*, 105.
(32) Goossens, W. J. A. *J. Phys.* **1979**, *40*, 158.